CAMBRIDGE
UNIVERSITY PRESS

RESEARCH ARTICLE

Lower limb exoskeleton for gait rehabilitation with adaptive nonsingular sliding mode control

Daniel Centeno-Barreda[1], Sergio Salazar-Cruz[1] (ID), Ricardo López-Gutiérrez[2],
Yukio Rosales-Luengas[1] and Rogelio Lozano[1]

[1]Center for Research and Advanced Studies of National Polytechnic Institute, Mexico City, Mexico
[2]CONACYT-CINVESTAV, Mexico City, Mexico
Corresponding author: Sergio Salazar-Cruz; Email: sesalazar@cinvestav.mx

Abstract

This paper introduces a lower limb exoskeleton for gait rehabilitation, which has been designed to be adjustable to a wide range of patients by incorporating an extension mechanism and series elastic actuators (SEAs). This configuration adapts better to the user's anatomy and the natural movements of the user's joints. However, the inclusion of SEAs increases actuator mass and size, while also introducing nonlinearities and changes in the dynamic response of the exoskeletons. To address the challenges related to the human–exoskeleton dynamic interaction, a nonsingular terminal sliding mode control that integrates an adaptive parameter adjustment strategy is proposed, offering a practical solution for trajectory tracking with uncertain exoskeleton dynamics. Simulation results demonstrate the algorithm's ability to estimate unknown parameters. Experimental tests analyze the performance of the controller against uncertainties and external disturbances.

1. Introduction

Exoskeletons for gait rehabilitation aim to restore the motor functions of individuals with gait impairments resulting from conditions such as stroke [1, 2], congenital disorders [3, 4], or neuromuscular injuries [5]. Their primary function is to assist patients in performing functional movements, thereby promoting brain plasticity, and aiding in their recovery. Additionally, sensors attached to the exoskeleton enable measurement and recording of the patient's forces and movements. The data obtained provides to the therapist with relevant information to evaluate the patient's progress and facilitates the design of specific rehabilitation programs customized to the patient's condition, which can improve the quality of rehabilitation and level of motor recovery.

The process of gait rehabilitation involves tracking predefined gait trajectories that can be adapted according to the patient's capabilities. Passive rehabilitation demands minimal patient participation and is particularly useful during the early stages of rehabilitation. In active rehabilitation, the exoskeleton introduces resistance to the movements of specific joints or muscle groups, creating a challenging environment for patients, consequently strengthening the muscles and enhancing coordination.

Flexible joint exoskeletons, composed of series elastic actuators (SEAs), offer additional advantages for rehabilitation [6, 7]. The elastic element provides flexibility, improving safety and comfort, resulting in a more organic walking assistance and better adaptation to anatomical differences and the natural movements of the patients. Moreover, by measuring the angular difference between the actuator and the elastic element, SEAs can serve as force sensors, which proves useful in the case of active rehabilitation. However, flexible joints also introduce additional nonlinearities and changes in the dynamic response, thereby increasing the complexity in determining the dynamics of the exoskeleton.

A major challenge to control exoskeletons is the human–machine dynamic interaction, for example, exoskeletons for active rehabilitation need to correct the user's motion when it diverges from the desired trajectory and simultaneously must contend with external disturbances (opposing forces caused by involuntary movements of the patient). Additionally, the dynamics of the exoskeleton are influenced by the presence of unmodeled dynamics and parametric uncertainties, stemming from the complexity of modeling human body dynamics and the variability in human anatomy. One way to address this problem is by implementing robust control algorithms.

Various control techniques have been proposed for the gait tracking control of exoskeletons, for example, assisted-as-needed control [8], which is focused on providing minimum necessary assistance for a patient to complete a movement. There are also model-based controllers, which require an exact knowledge of the dynamic parameters of the system [9, 10]. Other controllers do not require an accurate dynamic model or precise dynamic parameters, like proportional-integral-derivative (PID) control with particle swarm optimization [11], focused on optimizing the gain parameters. Other researchers have used optimization algorithms for dynamic parameter identification like particle swam optimization [12], beetle swarm optimization [13], and gait multi-objective optimization [14]. Also, it has been proposed some control algorithms that do not require knowledge of the system's dynamic model, such as model-free deep reinforcement learning [15], fuzzy radial-based impedance control [16], and dynamic movement primitives with reinforcement learning [17]. Other authors have proposed adaptive control strategies, for instance, in ref. [18], a fixed time sliding mode control is proposed to control nonlinear systems with external disturbances where the adaptive scheme is used to compensate for the unknown bounded external disturbances. In ref. [19], the authors propose an adaptive gain tuning algorithm, for time delay control. This schema provides fast and stable adaptation under significant payload change.

The present study focuses on tracking control for gait rehabilitation therapy using the lower limb exoskeleton, as shown in Figure 1. The prototype integrates an extension mechanism and SEAs. This design enhances adaptation to the user's anatomy and the natural motions of their joints. However, it also introduces parametric uncertainties related to the difficulty in accurately determining the user's parameters, as well as dynamic uncertainties associated with neglected or unknown dynamics derived from the elastic element. To address these challenges, an adaptive nonsingular terminal sliding mode control (ANTSMC) is proposed. This control strategy integrates an adaptive parameter adjustment strategy to deal with changes in the dynamics of the system associated with variations in human anatomy and the dynamic interaction with flexible joints in the exoskeleton, while also mitigating the effects of external disturbances. The controller's robustness against uncertainties and external disturbances is validated through numerical simulations and real-time experiments.

The main contribution of this study can be summarized as follows: (1) The development of an exoskeleton for gait rehabilitation, capable of adapting to the anatomical variations of each user, as well as sudden changes in system dynamics during the rehabilitation process, also showing robustness against external perturbations presented in the form of involuntary muscle contractions, ensuring that patients accurately follow gait movements during the entire rehabilitation therapy. (2) By implementing the nonsingular terminal sliding mode control, a practical solution is offered that reduces the complexity of the human–machine interaction involved in the rehabilitation of exoskeletons.

The paper is structured as follows: Section 2 describes the lower limb exoskeleton. Section 3 presents the exoskeleton's dynamic model as well as the human gait trajectory. Section 4 discusses the proposed ANTSMC, including its stability analysis. Section 5 presents simulation results, while Section 6 details the experimental validation of the proposed ANTSMC. General conclusions are provided in Section 7.

2. Exoskeleton description

The exoskeleton depicted in Figure 1 has been specifically designed for gait rehabilitation tasks and comprises two primary components: the lifting system and the lower limb system.

Table I. *Range of motion allowed by the exoskeleton.*

Joint	Minimum angle	Maximum angle	Link	Minimum length	Maximum length
Hip	-14°	90°	Hip to knee	0.33 m	0.43 cm
Knee	0°	110°	Knee to foot	0.40 m	0.53 cm
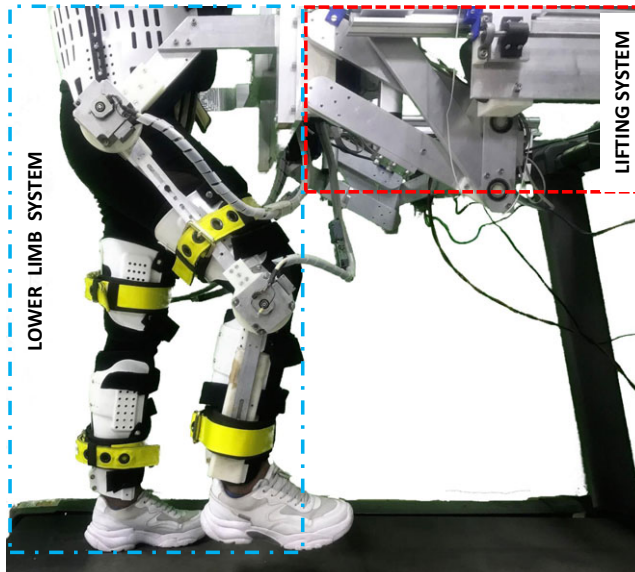
Figure 1. *Lower limb exoskeleton prototype configured in standing position.*

The lifting system is responsible for supporting the full weight of the patient, it features a twin four-bar system driven by two linear actuators, and its main function is to facilitate the transition from a seated to a standing position while ensuring the patient's vertical alignment. This support is maintained throughout the entire rehabilitation session leaving the lower limb system to only deal with the patient's legs.

The lower limb system is designed to be adjustable to the patient's legs from the front side, facilitating the process of fitting the exoskeleton while sitting in a wheelchair. Then, the lifting system assists the patient to stand up and start the gait rehabilitation. Four degrees of freedom (DoF) are allocated to the lower limbs, with each limb having two DoF located at the knee and hip joints. Considering the anatomical diversity among patients, an extension mechanism is incorporated into the thighs and lower legs links. For safety and to prevent hyperextension, the lower limb system was mechanically limited to the ranges, as shown in Table I. Each joint is operated by a series elastic actuator, which is composed of a torsional spring coupled between a harmonic drive motor model FHA-14C-100 and the exoskeleton's links, as illustrated in Figure 2. The torsional spring serves as the compliant element of the system, absorbing external forces and allowing the actuator to deform slightly, providing safety and comfort when interacting with patients. Additionally, each joint is equipped with two absolute encoders, model AMT20: one is utilized to detect the angular position of the motor shaft, while the second encoder measures the angular position of the link. The mechanical configuration of this prototype enables it to adapt to the user's anatomy and provide compliance with the natural movements of the user's joints. However, the elastic element introduces uncertainties that can significantly impact the dynamic behavior of the exoskeleton. Additionally the parametric variations among users result in a dynamic model with parametric uncertainties, thereby increasing the complexity in determining its exact dynamics.
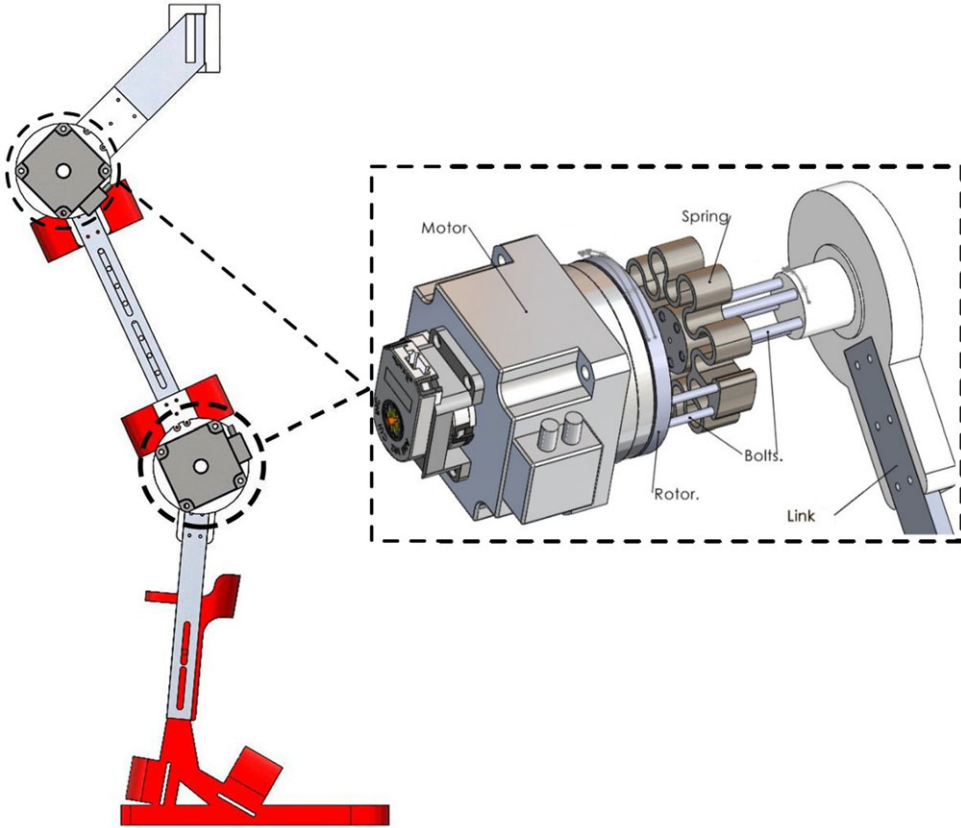
Figure 2. *Series elastic actuator mechanical configuration.*

3. Dynamic model

Figure 3 shows the simplified free body diagram of the lower limb system, where l_1 and l_2 correspond to the thigh and leg length, respectively. The distances to the center of mass of each link are represented by l_{c1} and l_{c2}, the mass of each link is specified by m_1 and m_2, and the inertia of each link is described by I_1 and I_2. The values corresponding to each parameter for the lower limb exoskeleton are presented in Table II. The dynamical model, expressed in compact form and obtained through the Euler–Lagrange approach, is as follows:

$$M(q)\ddot{q} + C(q,\dot{q})\dot{q} + g(q) + \delta(t) = \tau(t) + \tau_h(t) \tag{1}$$

with

$$M_{11} = I_1 + I_2 + l_{c1}^2 m_1 + (l_1^2 + l_{c1}^2 + 2l_1 l_{c2} \cos(q_2))m_2$$
$$M_{12} = I_2 + l_{c1}^2 m_2 + l_1 l_2 m_2 \cos(q_2)$$
$$M_{21} = I_2 + l_{c1}^2 m_2 + l_1 l_2 m_2 \cos(q_2)$$
$$M_{22} = I_2 + m_2 l_{c2}^2$$
$$C_{11} = -m_2 l_1 l_{c2} \sin(q_2)\dot{q}_2$$
$$C_{12} = -m_2 l_1 l_{c2} \sin(q_2)[\dot{q}_1 + \dot{q}_2]$$
$$C_{21} = m_2 l_1 l_{c2} \sin(q_2)\dot{q}_1$$
$$C_{22} = 0$$
$$G_1 = [m_1 l_{c1} + m_2 l_1]g \sin(q_1) + m_2 l_{c2} g \sin(q_1 + q_2)$$
$$G_2 = m_2 l_{c2} g \sin(q_1 + q_2)$$

Table II. *Exoskeleton parameters.*

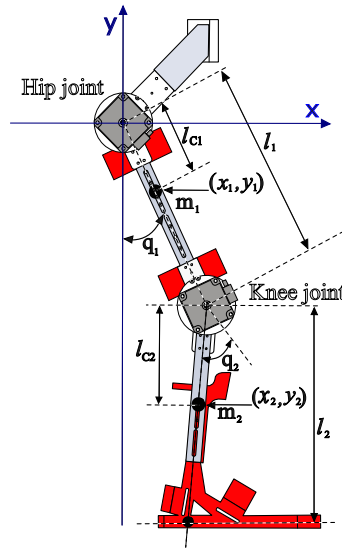| l_1	l_2	l_{c1}	l_{c2}	m_1	m_2	I_1	I_2	g
0.33	0.458	0.0741	0.04849	0.5272	0.6442	0.1213	0.116	9.81
m	m	m	m	Kg	Kg	Kgm^2	kgm^2	m/s^2

Figure 3. *Exoskeleton's free body diagram.*

where q, $\dot{q}$, and $\ddot{q} \in \mathbb{R}^2$ indicate the angular position, velocity, and acceleration, respectively. $M(q) \in \mathbb{R}^{2\times2}$ represents the inertia matrix, $C(q,\dot{q}) \in \mathbb{R}^{2\times2}$ denotes to the Coriolis and centripetal forces matrix, $G(q) \in \mathbb{R}^2$ corresponds to the vector of gravitational forces and torques, $\delta(t) \in \mathbb{R}^2$ symbolizes the unmodelled dynamics related to the elastic joint, while $\tau_h(t)$ denotes the external disturbances or involuntary movements of the user, and $\tau(t) \in \mathbb{R}^2$ represents the control input.

3.1. Trajectories for hip and knee joints

Prior to designing the controller, it is necessary to establish the gait trajectory. Human gait is a complex process of locomotion, which involves the forward movement of the human body in a bipedal stance. During this process, the weight is alternately supported by the lower limbs. The gait cycle occurs as one foot makes contact with the ground, and it continues until the same foot contacts the ground again [20]. This gait pattern can be modeled over the sagittal plane, as depicted in Figure 4.

The desired trajectories have been obtained by recording the gait of a healthy patient using the motion capture system *OptiTrack*, at 100 FPS, with a particular focus on the movements of the knee and hip joints. Through the analysis of the obtained data, the following paths for the hip and knee joints were determined:

$$q_{d1} = A(0.702 \sin(0.441p + 4.243) + 48.17 \sin(p + 4.816) + 1.68 \sin(2.998p - 0.02)$$

$$+ 1.634 \sin(0.361p + 2.314) + 17.2 \sin(0.086p + 0.241) + 69.61 \sin(p + 1.725)$$

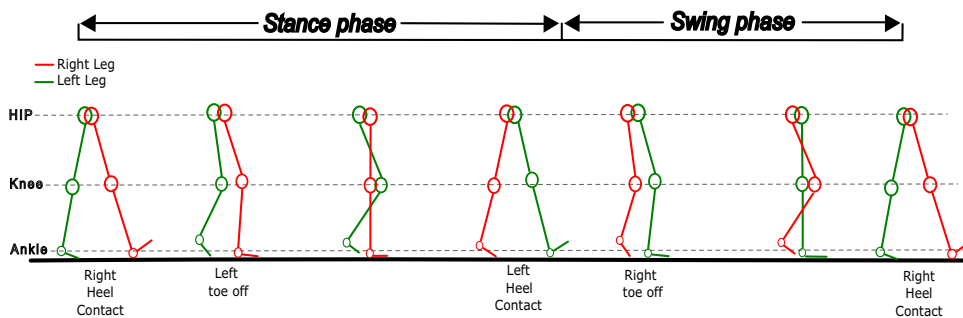$$+ 6.901 \sin(0.177p + 2) + 4 \sin(2p - 1.725)) \tag{2a}$$
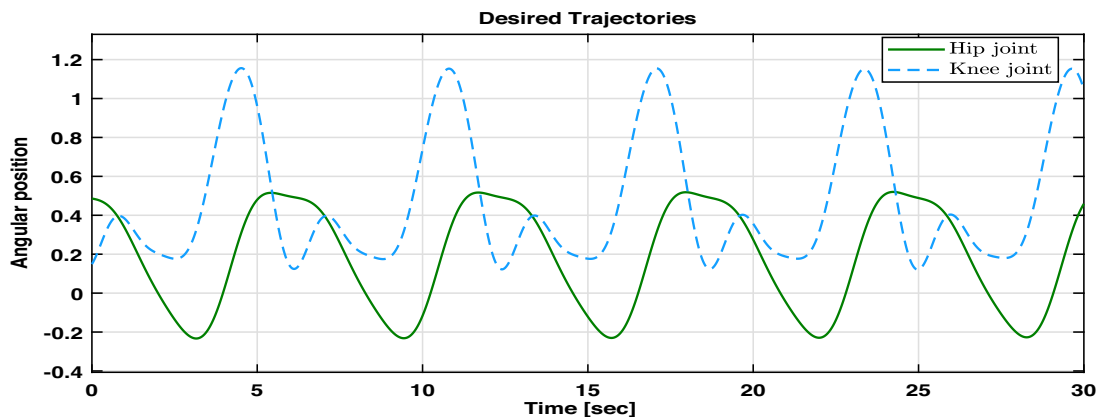
Figure 4. *Human gait cycle.*

Figure 5. *Desired trajectories obtained through the analysis of human gait.*

$$
\begin{aligned}
q_{d2} = A(&18.45\sin(0.351p+6) + 1.277\sin(3.989p-0.654) + 4.372\sin(3p-0.026) \\
&+ 20.92\sin(0.342p+2.98) + 44.71\sin(0.083p+0.366) + 21.13\sin(p-2.921) \\
&+ 16\sin(2p-0.95) + 20\sin(0.157p+2.446))
\end{aligned} \tag{2b}
$$

where q_{d1} and q_{d2} represent the knee and hip joints, respectively, while the parameters A and p are utilized to modify the walking speed and step length. Adjusting these parameters facilitates the development of personalized gait routines tailored to the unique needs of each patient. Figure 5 illustrates the trajectories for the hip and knee joints.

4. Control algorithm development

In this section, the proposed ANTSMC for the lower limb exoskeleton is developed. First, some important properties of the dynamic model of the exoskeleton are detailed, serving as the basis for the control algorithm development. Afterward, a nonsingular terminal sliding mode control is presented and the adaptive gain parameter adjustment strategy for the reaching law is developed to estimate the upper bound of uncertainties and disturbances, constructing the ANTSMC. The Lyapunov approach is employed to demonstrate the stability of the closed-loop system.

4.1. Preliminaries

Consider the dynamical model of the exoskeleton defined in (1). The control algorithm is designed taking into account that the system comprises both the user and the exoskeleton. Then, the model can

be divided into two parts: one representing the known value of the dynamics denoted by the subscript o and the other corresponding to the parametric uncertainties denoted by the subscript Δ, that is:

$$M(q) = M_o(q) + M_\Delta(q) \tag{3a}$$
$$C(q, \dot{q}) = C_o(q, \dot{q}) + C_\Delta(q, \dot{q}) \tag{3b}$$
$$g(q) = g_o(q) + G_\Delta(q) \tag{3c}$$

Then, Eq. (1) can be written in the following form:

$$M_0(q)\ddot{q} + C_0(q, \dot{q})\dot{q} + G_0(q) = \tau + \rho(t) \tag{4}$$

where $\rho(t) = -M_\Delta(q)\ddot{q} - C_\Delta(q, \dot{q}) - G_\Delta(q) - \delta + \tau_h$ represents the uncertainties of the system, including parametric uncertainties, external disturbances, and unmodeled dynamics of the flexible joint.

The exoskeleton can be considered as a chain of links connected in series by rotational joints. Consequently, it also satisfies some properties of boundedness in the dynamic model of revolute joint robots. Therefore, the following assumptions can be made.

Assumption 1. *There exist positive constants denoted as* α_i *such that the norms of the inertia matrix* $M(q)$, *the matrix representing Coriolis and centripetal forces* $C(q, \dot{q})$, *and the vector of gravitational forces and torque* $G(q)$ *satisfy* [21]:

$$||M(q)|| < \alpha_0 \tag{5a}$$
$$||C(q, \dot{q})\dot{q} + G(q)|| < \alpha_1 + \alpha_2||q|| + \alpha_3||\dot{q}||^2 \tag{5b}$$

Assumption 2. *The system uncertainty* $\rho(t)$ *is bounded by a function of the position and velocity measurements with positive constants* b_0, b_1, *and* b_2 *as follows:*

$$||\rho(t)|| < \begin{bmatrix} 1 & ||q|| & ||\dot{q}||^2 \end{bmatrix} \begin{bmatrix} b_0 & b_1 & b_2 \end{bmatrix}^T \triangleq Q\beta \tag{6}$$

These assumptions have been utilized by numerous researchers [22–24]. Assumption 1 is derived from the fundamental properties of dynamics boundedness in revolute joint robots. However, Assumption 2 implies that the magnitude of the upper bound of the exoskeleton uncertainties, denoted as ρ, is dependent on the system states. In other words, the magnitude of the uncertainties can vary according to the exoskeleton's dynamic response [25].

4.2. Adaptive nonsingular terminal sliding mode control

Let $\begin{bmatrix} q_d & \dot{q}_d \end{bmatrix}^T$ where q_d and $\dot{q}_d \in \mathcal{R}^2$ be the desired position and velocity for the exoskeleton hip and knee joints, and let the tracking error and its derivatives be defined as $\tilde{q} = q - q_d$, $\dot{\tilde{q}} = \dot{q} - \dot{q}_d$, and $\ddot{\tilde{q}} = \ddot{q} - \ddot{q}_d$, respectively. Then, using Eq. (4), the error dynamics can be expressed as:

$$\ddot{\tilde{q}} = M_0^{-1}(q)[\tau - C_0(q, \dot{q}) - G_0(q) + \rho(t) - M_0(q)\ddot{q}_d] \tag{7}$$

The control objective is to determine a control law τ that enables the exoskeleton output q to follow the desired trajectory $\begin{bmatrix} q_d & \dot{q}_d \end{bmatrix}^T$ and ensures that the tracking error converges to zero within a finite time. To achieve this goal, the nonsingular terminal sliding manifold is considered [26]:

$$s = \tilde{q} + K\dot{\tilde{q}}^{a/b} \tag{8}$$
$$\dot{s} = \dot{\tilde{q}} + K\frac{a}{b}diag(\dot{\tilde{q}}^{\frac{a}{b}-1})\ddot{\tilde{q}} \tag{9}$$

where $K = diag\{k_1, \ldots, k_n\}$ and a and b are odd integers satisfying $1 < a/b < 2$. The control law is chosen as:

$$\tau(t) = \tau_{eq}(t) + \tau_{sw}(t) \tag{10a}$$

$$\tau_{eq}(t) = C_0(q, \dot{q}) + G_0(q) + M_0(q)\ddot{q}_d$$
$$- \frac{b}{a}M_0(q)K^{-1}\dot{\tilde{q}}^{2-\frac{a}{b}} \tag{10b}$$

$$\tau_{sw}(t) = -\frac{[s^T K diag(\dot{\tilde{q}}^{\frac{b}{a}} - 1)M_0^{-1}(q)]^T}{\|s^T K diag(\dot{\tilde{q}}^{\frac{a}{b}} - 1)M_0^{-1}(q)\|}Q\beta \tag{10c}$$

The ANTSMC (10a) ensures the convergence of tracking error to equilibrium in finite time and robustness against uncertainties and disturbances. However, prior knowledge of the upper bound of system uncertainties (6) is required. Nevertheless, accurately estimating this upper bound can be challenging due to the interaction between the exoskeleton and the user. Uncertainties may be influenced by factors such as users' anatomical variability, as well as the nonlinear dynamics of human motion. Additionally, flexible joints introduce additional nonlinearities and changes in dynamic response. These characteristics can make it even more challenging to establish a precise upper bound for uncertainties in the system, complicating the implementation of this control algorithm. To address this problem, an adaptive parameter adjustment strategy is proposed for the reaching law (10c) to estimate $\beta = \begin{bmatrix} b_0 & b_1 & b_2 \end{bmatrix}^T$ online.

Theorem 1. *The exoskeleton represented by (1) and considering Assumptions 1 and 2, the following control algorithm:*

$$\tau(t) = \tau_{eq}(t) + \tau_\Delta(t) \tag{11a}$$

$$\tau_{eq}(t) = C_0(q, \dot{q}) + G_0(q) + M_0(q)\ddot{q}_d$$
$$- \frac{b}{a}M_0(q)K^{-1}\dot{\tilde{q}}^{2-\frac{a}{b}} \tag{11b}$$

$$\tau_\Delta(t) = -\frac{[s^T C_1 diag(\dot{\tilde{q}}^{\frac{a}{b}} - 1)M_0^{-1}(q)]^T}{\|s^T C_1 diag(\dot{\tilde{q}}^{\frac{a}{b}} - 1)M_0^{-1}(q)\|}Q\hat{\beta} \tag{11c}$$

where $\hat{\beta} = \begin{bmatrix} \hat{b}_0 & \hat{b}_1 & \hat{b}_2 \end{bmatrix}^T$ are the adaptive variables for b_0, b_1, and b_2 defined in (6). The adaptive law is:

$$\dot{\hat{\beta}} = \mu_1^{-1}Q^T\|s\| \tag{12}$$

And μ_1^{-1} is the adaptation gain that determines the rate of estimation. Then, the tracking error $[\tilde{q}, \dot{\tilde{q}}]^T$ will converge to zero in finite time.

Proof. Based on ref. [27], consider the following Lyapunov function:

$$V = \frac{1}{2}s^T s + \frac{1}{2}\mu_\beta \tilde{\beta}^T \tilde{\beta} \tag{13}$$

where $\tilde{\beta} = \beta - \hat{\beta}$ is the adaptive estimation error and $\mu_\beta > 0$. Differentiating V with respect to time and substituting Eqs. (7), (11a), (11b), and (11c) into it, we obtain the following:

$$\dot{V} = s^T\dot{s} - \mu_\beta \tilde{\beta}^T \dot{\hat{\beta}}$$
$$= s^T[\dot{\tilde{q}} + \frac{a}{b}K diag(\dot{\tilde{q}}^{\frac{a}{b}-1})\ddot{\tilde{q}}] - \mu_\beta \tilde{\beta}^T \dot{\hat{\beta}}$$
$$= s^T[\frac{a}{b}K diag(\dot{\tilde{q}}^{\frac{a}{b}-1})(M_0^{-1}(q)[\tau_\Delta + \rho])] - \mu_\beta \tilde{\beta}^T \dot{\hat{\beta}}$$
$$= -\|s^T\frac{a}{b}K diag(\dot{\tilde{q}}^{\frac{a}{b}-1})M_0^{-1}(q)\|Q\hat{\beta} + s^T\frac{a}{b}K diag(\dot{\tilde{q}}^{\frac{a}{b}-1})M_0^{-1}(q)\rho - \mu_\beta \tilde{\beta}^T \dot{\hat{\beta}} \tag{14}$$
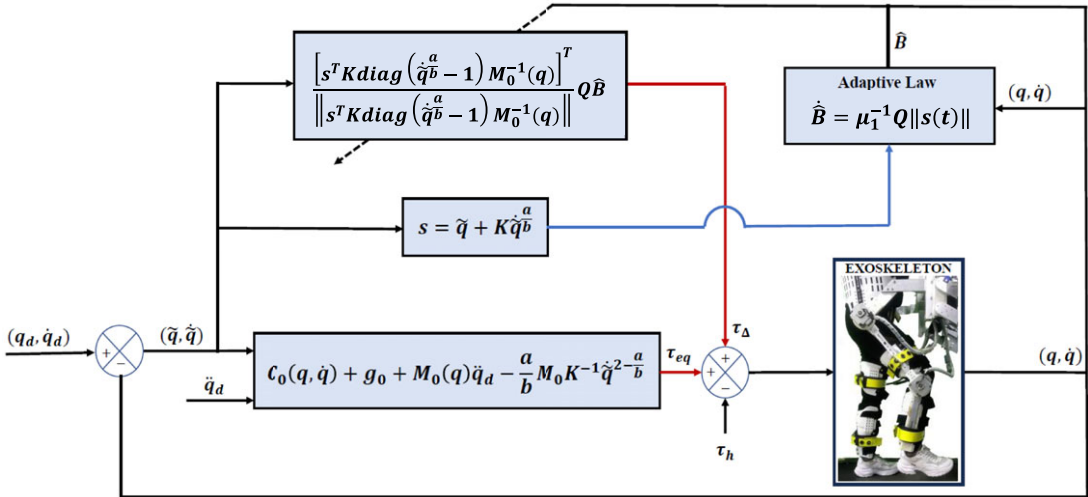
Figure 6. *Block diagram of the adaptive non-singular terminal sliding mode control.*

by substitution of the adaptive law defined in Eq. (12), we obtain:

$$\dot{V} = -\|s^T \frac{a}{b} Kdiag(\dot{\tilde{q}}^{\frac{a}{b}-1}) M_0^{-1}(q)\| Q\hat{\beta} + s^T \frac{a}{b} Kdiag(\dot{\tilde{q}}^{\frac{a}{b}-1}) M_0^{-1}(q)\rho - \mu_\beta \tilde{\beta}^T \mu_1^{-1} Q^T \|s\|$$

$$= -\|s^T \frac{a}{b} Kdiag(\dot{\tilde{q}}^{\frac{a}{b}-1}) M_0^{-1}(q)\| Q\hat{\beta} + s^T \frac{a}{b} Kdiag(\dot{\tilde{q}}^{\frac{a}{b}-1}) M_0^{-1}(q)\rho - \mu_\beta \mu_1^{-1} Q\tilde{\beta} \|s\| \tag{15}$$

where μ_β and μ_1 are positive constants. Note that in Eq. (15), we apply the following property: $x^T y = y^T x$ with $x = \tilde{\beta}$ and $y = Q^T$. In accordance with assumption (6) and by adding and subtracting $\frac{a}{b} \|Kdiag(\dot{\tilde{q}}^{\frac{a}{b}-1}) M_0^{-1}(q)\| \|\Lambda\beta\| \|s\|$, Eq. (14) can be simplified as follows:

$$\dot{V} \le \frac{a}{b} \|s\| \|Kdiag(\dot{\tilde{q}}^{\frac{a}{b}-1}) M_0^{-1}(q)\| (\|\rho\| - \|Q\hat{\beta}\|)$$

$$+ \frac{a}{b} \|Kdiag(\dot{\tilde{q}}^{\frac{a}{b}-1}) M_0^{-1}(q)\| \|Q\beta\| \|s\|$$

$$- \frac{a}{b} \|Kdiag(\dot{\tilde{q}}^{\frac{a}{b}-1}) M_0^{-1}(q)\| \|Q\beta\| \|s\|$$

$$- \mu_\beta \mu_1^{-1} (\|Q\beta\| - \|Q\hat{\beta}\|) \|s\|$$

$$\le -\frac{a}{b} \|s\| \|Kdiag(\dot{\tilde{q}}^{\frac{a}{b}-1}) M_0^{-1}(q)\| (\|Q\beta\| - \|\rho\|)$$

$$- (\mu_\beta \mu_1^{-1} - \frac{a}{b} \|Kdiag(\dot{\tilde{q}}^{\frac{a}{b}-1}) M_0^{-1}(q)\|) \times$$

$$\|s\| (\|Q\beta\| - \|Q\hat{\beta}\|)$$

$$\le -\varphi_1 \sqrt{2} \frac{\|s(t)\|}{\sqrt{2}} - \varphi_2 \sqrt{\frac{2}{\mu_\beta}} \|\tilde{\beta}\| \sqrt{\frac{\mu_\beta}{2}}$$

$$\le \varphi_{min} \left(\frac{\|s(t)\|}{\sqrt{2}} + \sqrt{\frac{\mu_B}{2}} \|\tilde{\beta}\| \right)$$

$$\le -\varphi_{min} V^{\frac{1}{2}} \tag{16}$$

where

$$\varphi_1 = \frac{a}{b} \| K diag(\dot{\tilde{q}}^{\frac{a}{b}-1}) M_0^{-1}(q) \| (\| Q\beta \| - \| \rho \|)$$

$$\varphi_2 = \left(\mu_P \mu_1^{-1} - \frac{a}{b} \| K diag(\dot{\tilde{q}}^{\frac{a}{b}-1}) M_0^{-1}(q) \| \right) \| s(t) \| \| Q \|$$

$$\varphi_{min} = min \left(\varphi_1 \sqrt{2}, \ \varphi_2 \sqrt{\frac{2}{\mu_\beta}}, \right)$$

Hence, the proof shows that by using the adaptive parameters $\hat{\beta} = \begin{bmatrix} \hat{b}_0 & \hat{b}_1 & \hat{b}_2 \end{bmatrix}^T$, the stability is ensured, and the system reaches $s = 0$ in finite time. According to the Lemma 1 presented in ref. [27], the corresponding finite time t_r can be calculated as:

$$t_r \leq \frac{2V^{1/2}(t_0)}{\varphi} \tag{17}$$

According to ref. [26], when $s = 0$ is reached, the system dynamics are determined by $\tilde{q} + K\dot{\tilde{q}}^{a/b} = 0$. By solving this differential equation, the finite time t_s that the tracking error takes to reach the origin $\tilde{q}(t_s + t_r) = 0$ from $\tilde{q}(t_r) \neq 0$ is given by:

$$t_s = -K^{b/a} \int_{\tilde{q}(t_r)}^{\tilde{q}(t_r+t_s)} \frac{d\tilde{q}}{\tilde{q}^{b/a}} = K^{b/a} \frac{a}{a-b} \tilde{q}(t_r)^{(1-b/a)} \tag{18}$$

Finally, we can conclude that the nonsingular manifold $s = 0$ is reached in finite time. Furthermore, the tracking error also converges to zero in finite time. The closed-loop diagram of the ANTSMC is shown in Figure 6.

5. Numerical simulation results

The performance of the ANTSMC is evaluated through numerical simulation using the dynamics of the exoskeleton described in Eq. (4). The known dynamics, denoted as $M_0(q)$, $C_0(q, \dot{q})$, and $g_0(q)$, are obtained by considering an uncertainty of 20% with respect to the values presented in Table II. Initial conditions are selected as $\begin{bmatrix} q_1(0) & q_2(0) \end{bmatrix}^T = \begin{bmatrix} -0.2 & 0 \end{bmatrix}^T$ and $\begin{bmatrix} \dot{q}_1(0) & \dot{q}_2(0) \end{bmatrix}^T = \begin{bmatrix} 0 & 0 \end{bmatrix}^T$.

The discontinuous term τ_Δ can result in a chattering problem, which in practical applications may cause damage to system components such as actuators. To mitigate this undesirable effect, the boundary layer method is applied in (11c), resulting in the following expression:

$$\tau_\Delta = \begin{cases} \frac{s}{\eta} \Lambda \hat{\beta} & \text{if } \| s \| \leq \eta, \\ \frac{[s^T C_1 diag(\dot{\tilde{q}}^{\frac{a}{b}} - 1) M_0^{-1}(q)]^T}{\| s^T C_1 diag(\dot{\tilde{q}}^{\frac{a}{b}} - 1) M_0^{-1}(q) \|} \Lambda \hat{\beta} & \text{if } \| s \| > \eta \end{cases} \tag{19}$$

where η is a design parameter that determines the width of the boundary layer. By implementing the boundary layer method, the controller's sensitivity to uncertainties and external disturbances within the region defined by η is reduced, resulting in a nonzero tracking error. Furthermore, this expression leads to parameter drifting of the adaptive law $\dot{\hat{\beta}}$. To mitigate this issue, the dead-zone method is employed. As a result, the adaptive law (12) is reformulated as follows:

$$\dot{\hat{\beta}} = \begin{cases} 0 & \text{if } \| s \| \leq \epsilon, \\ \mu_1^{-1} \Lambda^T \| s \| & \text{if } \| s \| > \epsilon \end{cases} \tag{20}$$

where $\epsilon > 0$ represents the size of the dead zone.

The selected parameters for simulation are $a = 5$, $b = 3$, and $K = diag(0.3 \ 0.2)$. To maintain a small boundary layer while preserving the controller's sensitivity to uncertainties and external disturbances, η is set to 0.02. Figures 7 and 8 demonstrate the tracking performance of the hip and knee joints, respectively. Additionally, Figure 9 shows the control inputs with reduced chattering. In order to have a fast
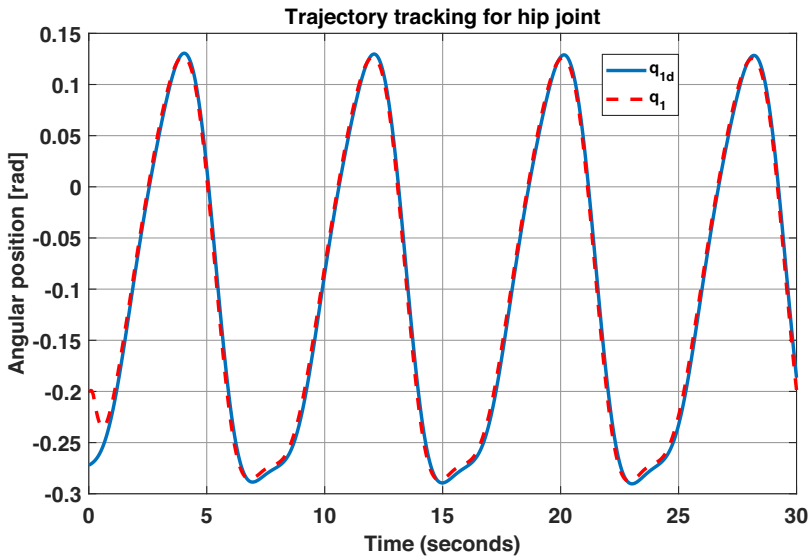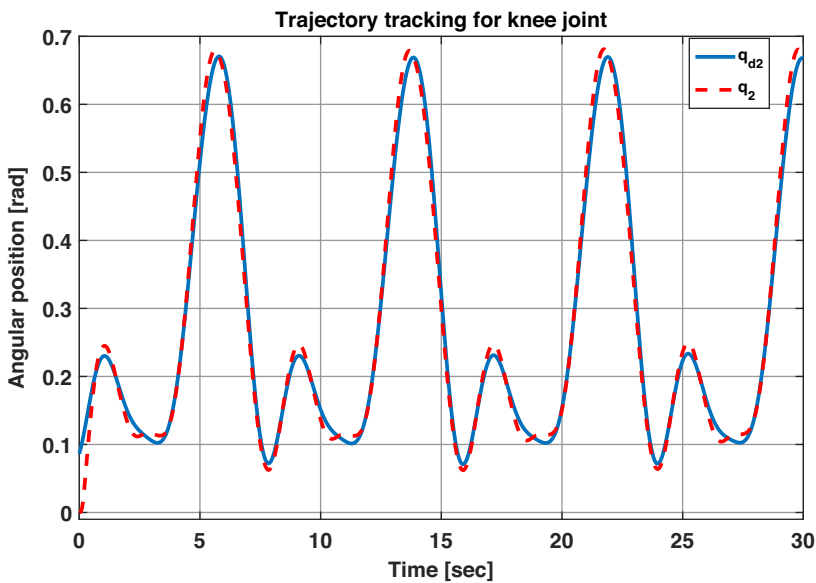
Figure 7. *Hip joint trajectory tracking.*

Figure 8. *Knee joint trajectory tracking.*

estimation of the adaptive parameters, μ_1 is set to 0.1 and $\epsilon = 0.06$. Figure 10 shows the performance of the parameters estimation for the upper bound of the uncertainties and external disturbances.

5.1. Performance comparison

The developed ANTSMC is compared with a proportional derivative (PD) controller, a conventional sliding mode controller (SMC), and an adaptive integral terminal sliding mode controller (AITSMC) [24] defined, respectively, as:
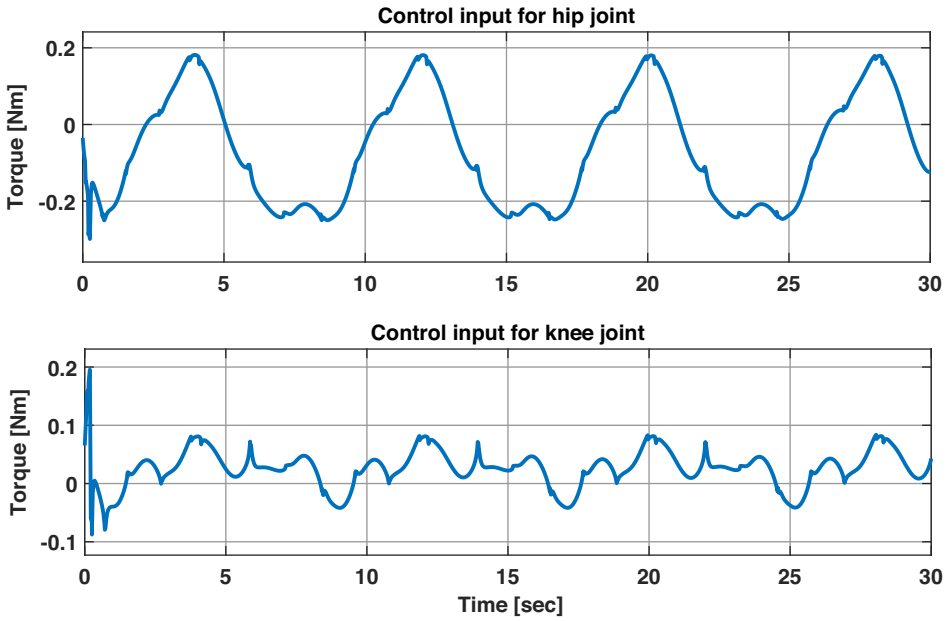
Figure 9. *Control inputs.*
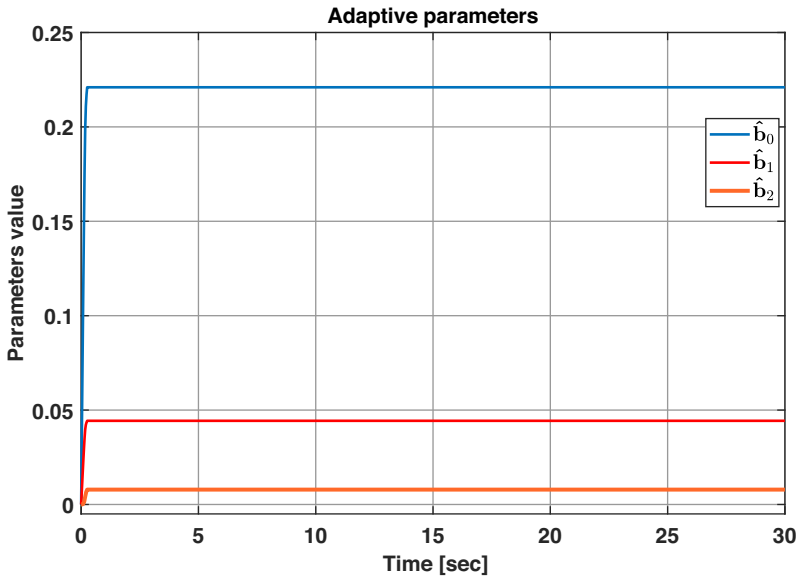
Figure 10. *Adaptive parameters estimation.*

$$\tau = K_p q + K_v \dot{q} \tag{21}$$

$$s = \dot{q} + Kq \tag{22}$$

$$s = \dot{q} + \int \alpha \dot{\tilde{q}}^{a/b} + \beta \tilde{q}^{a/2b-a} dt \tag{23}$$

For the PD controller, the gains were selected heuristically as $K_P = diag\left(15\ 8\right)$ and $K_d = diag\left(5\ 2\right)$. In the case of the SMC, $K = diag\left(4\right)$ and the upper bound of uncertainties as $\beta = \begin{bmatrix} 3\ 2\ 0.5 \end{bmatrix}^T$. The

Table III. *RMSE for each control strategy.*

	PD	**SMC**	**AITSMC**	**ANTSMC**
Hip	0.0215	0.0148	0.0192	0.0142
Knee	0.0231	0.0213	0.0274	0.0155
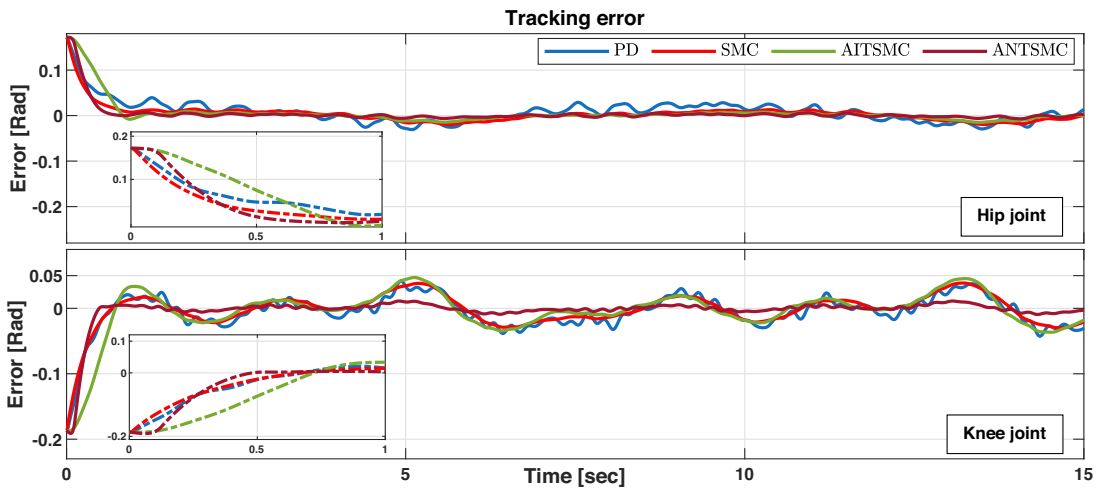
Figure 11. *Comparison of the tracking errors.*

parameters for the AITSMC are $\alpha = diag\,(3)$ and $\beta = diag\,(4)$, $a = 5$, $b = 3$, $\lambda = diag\,(100\ 300)$, and $\Gamma = diag\,(300)$. For all controllers, initial conditions are $q(0) = \begin{bmatrix} -0.1 & -0.1 \end{bmatrix}^T$ and $\dot{q}(0) = \begin{bmatrix} 0 & 0 \end{bmatrix}^T$. External disturbances are selected as $d = \begin{bmatrix} 0.72sin(10t)sin(t) & 0.55sin(25t)cos(2t) \end{bmatrix}^T$. For the SMC and AITSMC, the chattering effect is suppressed by using the boundary layer method. Figure 11 shows the tracking errors for the hip and knee joints. It can be noticed that all four controllers completed the trajectory tracking. However, the proposed ANTSMC presents a faster convergence rate and robustness against external perturbations. Table III shows the root mean square error (RMSE) for each controller. The obtained results prove the efficacy of the proposed controller.

Figure 12 shows the trajectory tracking response with different gains. It can be noted that with smaller gains, the convergence to the desired trajectory is faster. These results coincide with the finite time calculation described in Eq. (18), where the time at which $\tilde{q}(t) = 0$ is proportional to the gains.

6. Experimental results

The performance of the proposed ANTSMC against uncertainties and external disturbances is evaluated through a series of experimental tests conducted using the exoskeleton, as shown in Figure 1. For experimental purposes, the prototype has been configured to operate under two distinct scenarios. In the first scenario, the actuators are directly coupled to the exoskeleton's links, allowing for a rigid joint control approach. In contrast, the second scenario features a setup in which each joint is driven by the series elastic actuators, as depicted in Figure 2.

For the evaluation process, specific parameters have been chosen to tune the closed-loop system. The selected parameters for the controller are as follows: $a = 5$, $b = 3$, and $K = diag\,(3\ 1)$. Furthermore, for the boundary layer and adaptive law: $\eta = 0.2$, $\mu_1 = 3$, and $\epsilon = 0.06$. These parameter settings have been carefully selected to not only mitigate chattering in the control signal but also to maintain a trade-off
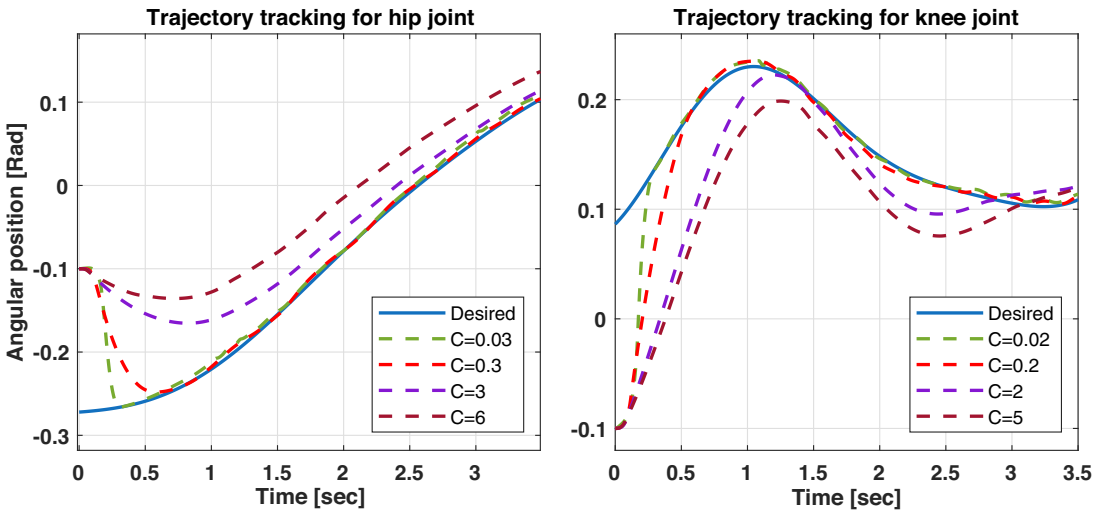
Figure 12. *Comparison of the trajectory tracking with different gains.*

between system performance and robustness. Additionally, the known dynamics, denoted as $M_0(q)$, $C_0(q, \dot{q})$, and $g_0(q)$, are obtained from Table II.

6.1. Experimental results with rigid joints

In this experimental test, the FHA-14C-100 actuators are directly coupled to the exoskeleton's links, and angular positions are measured using an ATM20 encoder. In this configuration, factors such as friction, gear inertia, and human dynamics are considered unknown. Figures 13 and 14 demonstrate that the trajectory tracking for the hip and knee joints is accurate, showcasing the effectiveness of the control strategy. Figure 15 shows the control signal with reduced chattering, ensuring the protection of the actuators from damage. During the time interval from $t = 0$ to $t = 9$, the amplitude of the desired trajectories was varied from $A = 0$ to $A = 0.3$. Additionally, at time $t = 25.5$, an external disturbance was introduced by applying an external force to the knee joint while it was in motion. These actions resulted in significant changes in the bounds of the unknown system dynamics, leading to corresponding adjustments in parameter estimation, as depicted in Figure 16.

6.2. Experimental results with elastic joints

This section demonstrates the effectiveness of the ANTSMC controller by extending the analysis to a configuration using series elastic actuators, as illustrated in Figure 2. This configuration is of special interest because it adapts better to the user's anatomy and the natural movements of the user's joints. Additionally, it enables the detection of user movement intentions by monitoring the angular position difference between the actuator and the link. However, the elastic element also introduces an additional uncertainties, which can significantly impact the dynamic behavior of the exoskeleton.

Typically, analyses of elastic joint robots assume uniform stiffness for all elastic elements. However, to increase the system's uncertainties, the torsional spring stiffness for the hip and knee joints differs. Specifically, for the hip joint, the stiffness is 10 Nm/grad, and for the knee joint, it is 30 Nm/grad. In this test, all phenomena related to the elastic elements, as well as the dynamics of the human user and its parameters, are considered unknown.

The performance analysis of ANTSMC to this configuration is particularly interesting, as it reflects the challenges encountered in practical scenarios where exoskeletons interact with the wearer's
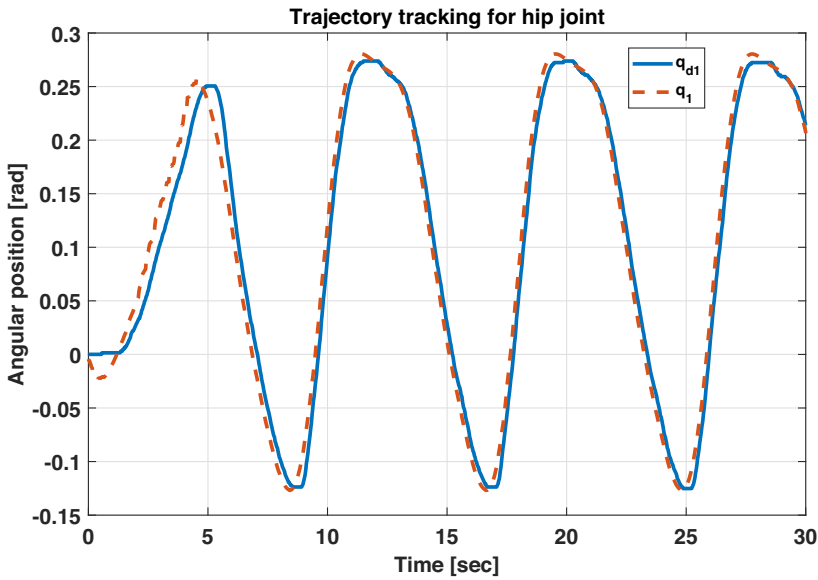
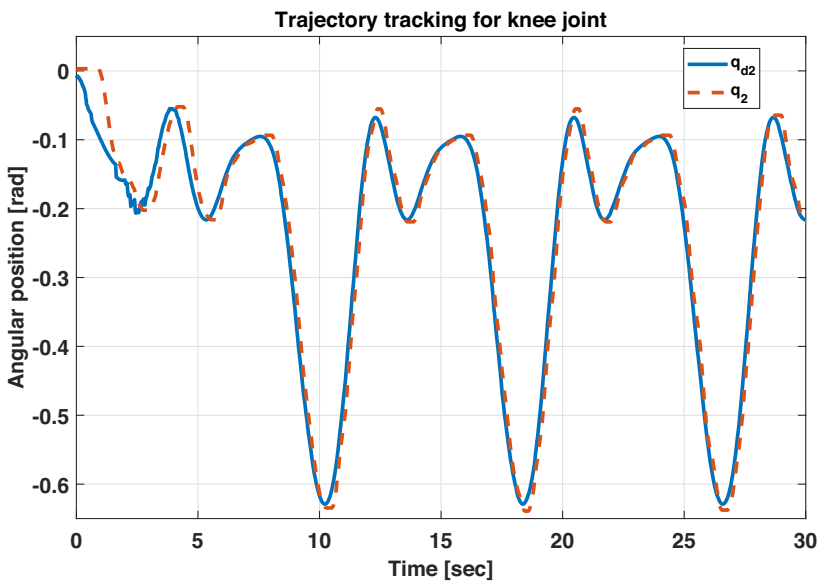**Figure 13.** *Hip joint trajectory tracking.*

Figure 14. *Knee joint trajectory tracking.*

movements. This includes situations where users have different parameters and each elastic joint varies its stiffness based on the wearer's strength.

Figures 17 and 18 show the trajectory tracking for the hip and knee joints. In these figures, q_{m1} and q_{m2} represent the angular displacement of the actuators, while q_{l1} and q_{l2} represent the angular displacement of the links. In both figures, three lines can be observed. The solid blue line represents the desired trajectory. The dotted red line shows the position of the link, and finally, the dashed green line represents the actuator's trajectory. It can be noted that the angular position of the motor differs from the desired position. This phenomenon is due to the elastic nature of the exoskeleton's joint and the transmission of motion. When the actuator drives the movement, it is initially transmitted to the spring, which needs
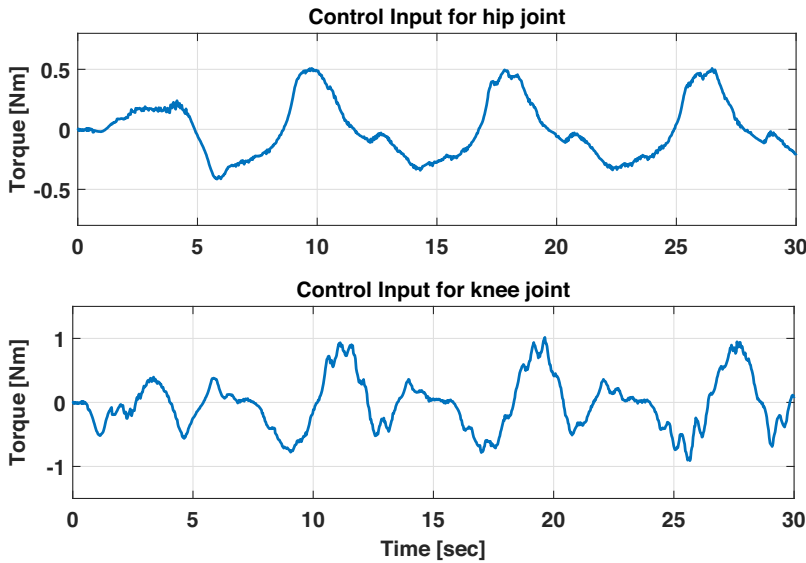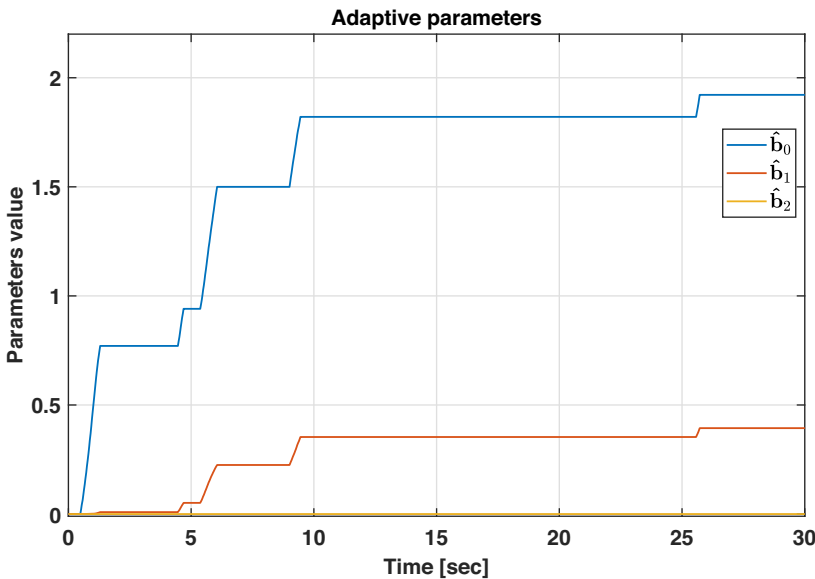
Figure 15. *Control inputs.*

Figure 16. *Adaptive parameters estimation.*

to deform to transmit the motion to the link. This causes a delay or phase lag in the response. This phenomenon can be clearly observed in Figure 17. Here, the elastic element of the hip has lower stiffness, causing greater deformation of the spring. As a result, the difference in angular displacement between the motor q_{m1} and the link q_{l1} is more noticeable, unlike the knee joint, in which the stiffness is higher, leading to less deformation of the spring. Consequently, the angular displacement of the motor q_{m2} is close to the angular displacement of the link q_{l2}, as shown in Figure 18. Another important aspect to detail is the correct tracking of the links q_{l1} and q_{l2} and the desired trajectories q_{d1} and q_{d2}. These results showcase the effectiveness of ANTSMC in flexible joint exoskeletons. Finally, Figs. 19 and 20 show the control signal and the real-time estimation of the upper bound of uncertainties.
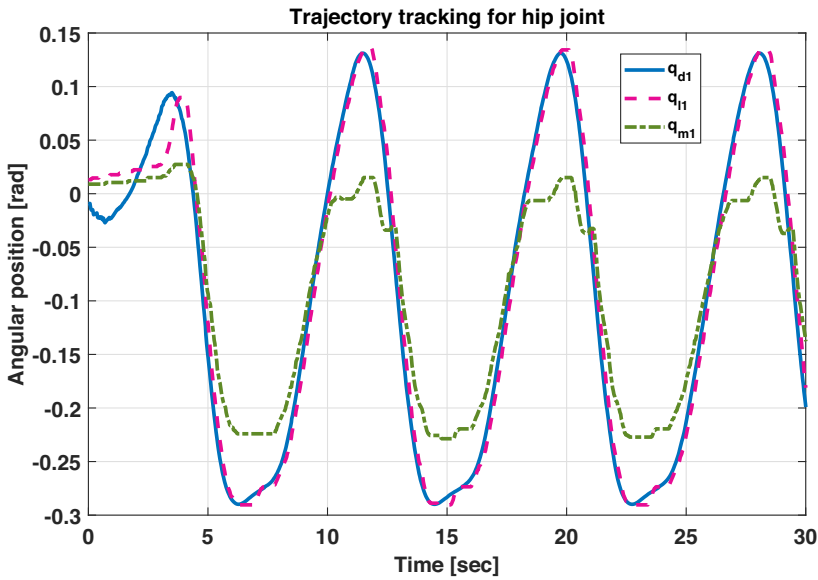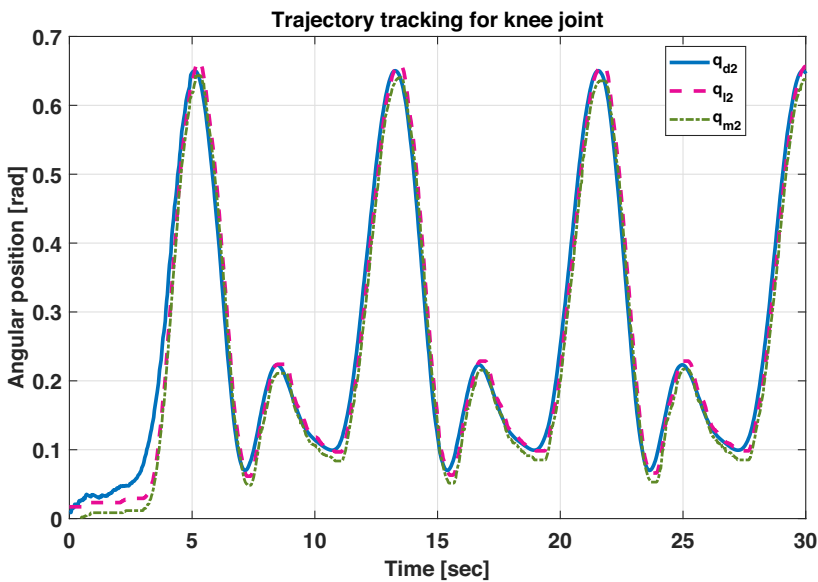
Figure 17. *Hip joint trajectory tracking.*

Figure 18. *Knee joint trajectory tracking.*

7. Conclusions

The lower limb exoskeleton introduced in this study is designed to adapt to the anatomical variations of each user and actively respond to sudden changes in system dynamics during the rehabilitation process. Additionally, by integrating elastic joints, the exoskeleton provides compliance, safety, and comfort during interactions with patients, ensuring accurate gait movement tracking throughout the entire rehabilitation therapy.

The proposed adaptive ANTSMC addresses the challenges posed by the variability in human anatomy and the dynamic interaction between the exoskeleton and the user, characterized by parametric uncertainties and the complexity of modeling human limb dynamics.
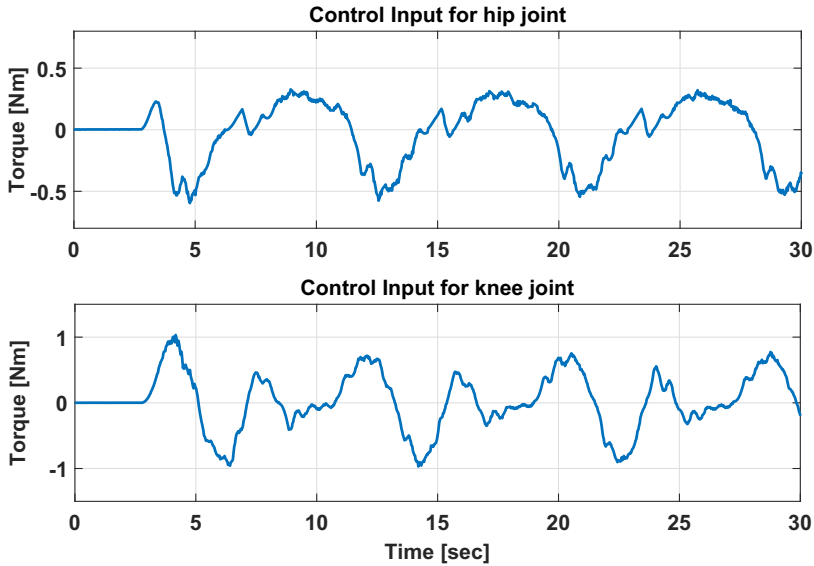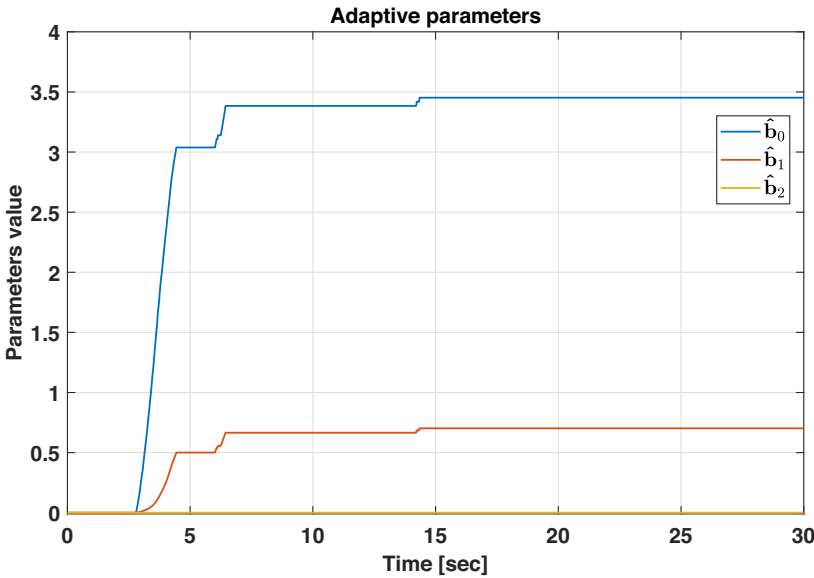
Figure 19. *Control inputs.*

Figure 20. *Adaptive parameters estimation.*

Simulation results validate the algorithm's capability to estimate the upper bound in real time and ensure the tracking of the human gait. Experimental tests were initially conducted with rigid joints and subsequently extended to a system with elastic joints. The experimental results further confirm the controller's suitability for rehabilitation purposes, guaranteeing both accurate trajectory tracking and robustness against uncertainties and external disturbances making it a robust solution for exoskeleton control in practical applications.

References

[1] E. Høyer, A. Opheim and V. Jørgensen, "Implementing the exoskeleton ekso gttm for gait rehabilitation in a stroke unit–feasibility, functional benefits and patient experiences," *Disabil. Rehabil. Assist. Technol.*, **17**, 473–479 (2022).

[2] D. Calafiore, F. Negrini, N. Tottoli and F. Ferraro, "Ozden Ozyemisci-Taskiran, etal, Efficacy of robotic exoskeleton for gait rehabilitation in patients with subacute stroke: A systematic review," *Eur. J. Phys. Rehab. Med.* **58**, 1–8 (2022).

[3] Y. Zhang, S. De Groof, L. Peyrodie and L. Labey, "Mechanical Design of an Exoskeleton with Joint-Aligning Mechanism for Children with Cerebral Palsy," **In:** *8th IEEE RAS/EMBS International Conference for Biomedical Robotics and Biomechatronics (BioRob)*, New York, USA (2020) pp. pages 106–111.

[4] D. Lee, M. K. Shepherd, S. C. Mulrine, J. D. Schneider, K. F. Moore, E. M. Eggebrecht, B. M. Rogozinski, K. R. Herrin and A. J. Young, "Reducing knee hyperextension with an exoskeleton in children and adolescents with genu recurvatum: A feasibility study," *IEEE. Trans. Bio-MED. Eng.* **70**, 3312–3320 (2023).

[5] S.-Y. Lee, C.-H. Seo, Y.-S. Cho and S.-Y. Joo, "Clinical utility of robot-assisted gait training in patients with spinal cord injury caused by electrical burns: A case report," *J. Clin. Med.* **112**, 7220 (2023).

[6] S. V. Sarkisian, L. Gabert and T. Lenzi, "Series-elastic actuator with two degree-of-freedom pid control improves torque control in a powered knee exoskeleton," *Wearable Technol.* **4**, e25 (2023).

[7] B. Zhong, K. Guo, H. Yu and M. Zhang, "Toward gait symmetry enhancement via a cable-driven exoskeleton powered by series elastic actuators," *IEEE Robot. Auto. Letters* **7**,786–793 (2022).

[8] C. Zou, C. Zeng, R. Huang, Z. Peng, J. Zhang and H. Cheng, "Online gait learning with assist-as-needed control strategy for post-stroke rehabilitation exoskeletons," *Robotica* **42**, 319–331 (2024).

[9] Y. Rosales-Luengas, K. I. Espinosa-Espejel, R. Lopéz-Gutiérrez, S. Salazar and R. Lozano, "Lower limb exoskeleton for rehabilitation with flexible joints and movement routines commanded by electromyography and baropodometry sensors," *Sensors* **23**, 5252 (2023).

[10] B. Liu, Y. W. Liu, Z. Zhou and L. Xie, "Control of flexible knee joint exoskeleton robot based on dynamic model," *Robotica* **40**, 2996–3012 (2022).

[11] J. Liu, H. Fang and J. Xu, "Online adaptive pid control for a multi-joint lower extremity exoskeleton system using improved particle swarm optimization," *Machines* **10**, 21 (2021).

[12] H. Tiaiba, M. E. H. Daachi and T. Madani, "Real-time adaptive super twisting algorithm based on PSO algorithm: Application for an exoskeleton robot," *Robotica* **42**, 1–26 (2024).

[13] P. Zhang and J. Zhang, "Lower limb exoskeleton robots' dynamics parameters identification based on improved beetle swarm optimization algorithm," *Robotica* **40**, 2716–2731 (2022).

[14] P. Zhang, J. Zhang and A. Elsabbagh, "Gait multi-objectives optimization of lower limb exoskeleton robot based on bso-eollff algorithm," *Robotica* **41**, 174–192 (2023).

[15] L. Rose, M. C. F. Bazzocchi and G. Nejat, "A model-free deep reinforcement learning approach for control of exoskeleton gait patterns," *Robotica* **40**, 2189–2214 (2022).

[16] P. Zhang, J. Zhang and A. Elsabbagh, "Fuzzy radial-based impedance controller design for lower limb exoskeleton robot," *Robotica* **41**, 326–345 (2023).

[17] P. Zhang and J. Zhang, "Motion generation for walking exoskeleton robot using multiple dynamic movement primitives sequences combined with reinforcement learning," *Robotica* **40**, 2732–2747 (2022).

[18] S. Ahmed, A. T. Azar and I. K. Ibraheem, "Nonlinear system controlled using novel adaptive fixed-time SMC," *AIMS Math.* **9**, 7895–7916 (2024).

[19] J. Lee, P. H. Chang and M. Jin, "An adaptive gain dynamics for time delay control improves accuracy and robustness to significant payload changes for robots," *IEEE. Trans. Ind. Electron.* **67**, 3076–3085 (2019).

[20] A. Kharb, Y. K. J. Vipin Saini and S. Dhiman, "A review of gait cycle and its parameters," *IJCEM Int. J. Comp. Eng. Mgmt.* **13**, 78–83 (2011).

[21] R. Kelly, V. S.áñez Davila and J. A. L.ía Perez. *Control of Robot Manipulators in Joint Space* (Springer, 2005).

[22] E. A. A. Salcido, D. Centeno-Barreda, Y. Rosales, R. López-Gutiérrez, S. Salazar and R. Lozano, "Design of a lower limb exoskeleton: Robust control, simulation and experimental results," *Algorithms* **16**, 449 (2023).

[23] L. Zhang, Y. Wang, Y. Hou and H. Li, "Fixed-time sliding mode control for uncertain robot manipulators," *IEEE Access* **7**, 149750–149763 (2019).

[24] A. Riani, T. Madani, A. Benallegue and K. Djouani, "Adaptive integral terminal sliding mode control for upper-limb rehabilitation exoskeleton," *Control Eng. Pract.* **75**, 108–117 (2018).

[25] M. Zhihong and X. Yu, "Adaptive terminal sliding mode tracking control for rigid robotic manipulators with uncertain dynamics," *JSME Int. J. Series C Mech. Sys., Mach. Elements Manuf.* **40**, 493–502 (1997).

[26] Y. Feng, X. Yu and Z. Man, "Non-singular terminal sliding mode control of rigid manipulators," *Automatica* **38**, 2159–2167 (2002).

[27] S. Ahmed, H. Wang and Y. Tian, "Adaptive fractional high-order terminal sliding mode control for nonlinear robotic manipulator under alternating loads," *Asian J. Control.* **23**, 1900–1910 (2021).